J Mol Model (2015) 21: 168
DOI 10.1007/s00894-015-2703-4

ORIGINAL PAPER

Specific distributions of anions and cations of an ionic liquid through confinement between graphene sheets

Mahtab Alibalazadeh[1] · **Masumeh Foroutan**[1]

Received: 10 January 2015 / Accepted: 17 May 2015 / Published online: 7 June 2015

Abstract This work was aimed to investigate the behavior, morphology, structure, and dynamical properties of pure ionic liquid (IL) 1-ethyl-3-methylimidazolium tetrafluoroborate ([emim][BF_4]) confined between two parallel and flat graphene sheets at different interwall distances, H. Thus, molecular dynamic (MD) simulations were performed for different interwall distances including (10, 14, 16, 20, 23, and 28) Å at seven temperatures from 278 to 308 K. These results showed that the distribution and orientation of cations and anions on the graphene sheets depended on H. At the shortest H, a dense monolayer of the anions and cations was formed between two graphene sheets. The number of these layers increased as H increased. The potential energy diagram as a function of H demonstrated a minimum potential energy at H=16 Å. Also, there was a minimum overlap between the density profiles of the cations and anions at H=16 Å. Diffusion coefficients of the cations and anions increased as temperature and H increased. Moreover, slope of the plot of the diffusion coefficients of the cations and anions versus H significantly changed at H=16 Å. Orientation functions revealed that most of the cations oriented parallel to the graphene sheets.

Keywords Confined · Graphene · Ionic liquid · Molecular dynamics simulation

Electronic supplementary material The online version of this article (doi:10.1007/s00894-015-2703-4) contains supplementary material, which is available to authorized users.

✉ Masumeh Foroutan
foroutan@khayam.ut.ac.ir

[1] Department of Physical Chemistry, School of Chemistry, College of Science, University of Tehran, Tehran, Iran

Introduction

Confined systems have attracted considerable interest in recent decades due to their different properties compared with bulk systems [1–3]. Study of these systems has become an important area of research with potential applications as development of new nanoscale devices. On the other hand, room temperature ionic liquids (RTILs) [4, 5] as new designing materials have been recently considered as an alternative solvent with many interesting qualities. For many of the electrochemical applications, Ills are promising for supercapacitors, batteries, and solar cells [6–10]. Therefore, it is important to have a fundamental understanding about the characteristics of the confined ILs. Investigations of the interfaces of the ILs, both solid and liquid, have been carried out using both experimental and simulation studies [11–18]. Recently, structure of the electrical double layer in IL 1-butyl-3-methylimidazolium hexafluorophosphate [BMIM][PF_6] near a charged and uncharged graphite surface has been studied [19]. The obtained results showed that the structure of the IL [BMIM][PF_6] differed from that of the bulk ones. Also, the imidazolium ring of the cation arranges parallel to the graphite surface in the first adsorption layer. Via MD simulations, the effects of the alkyl chain lengths of the IL cation on the interface between the ILs and graphite surface were investigated [20]. Results of this investigation showed that the imidazolium rings and the side chains of the cation preferred flat arrangement at the graphite surface. In addition to the above–mentioned studies, several reports have also reflected the properties of ILs on the graphite surfaces [21–23].

Recently, composites of graphene and ILs have received great attention [24, 25]. Ariga et al. [26, 27] introduced a method for preparing the composites of graphene/ILs and the subsequent layer-by-layer assembly that have practical applications for the capture of gases and as sensors [28]. Also,

IL–stabilized graphene has been used in immobilizing metal nanocatalysts [29]. Some attempts have been made to investigate the structure and dynamics of the ILs confined inside graphene and carbon nanotubes [30–33]. Using atomistic MD simulations, Wu et al. showed that confinement can result in an unusual behavior in the properties of ILs [34]. Hung et al. investigated the effect of diameter of the multiwalled carbon nanotubes and the pore loading on the properties of the IL [BMIM][PF_6] [33]. Kohanoff et al. [35] simulated the molten salt 1,3-dimethylimidazolium chloride confined between two flat parallel walls and showed a structure of layers parallel to the walls. Recently, Rajupt et al. [30, 32] performed MD simulations of the 1-ethyl-3-methylimidazolium bis-(trifluoromethanesulfonyl) imide IL inside a rutile (110) slit nanopore and a slit graphitic nanopore. They found that the interactions between the IL and surface affected the properties of the confined IL. Kim et al. [31] studied the supercapacitors consisting of two single-sheet graphene electrodes and found that, in contrast to emim, anion was more efficient in shielding electrode charges. Recently, [emim][BF_4] has been investigated in some experimental and theoretical studies [36–41]. Singh et al. [37] demonstrated that phase transition temperatures and thermal stability of [emim][BF_4] on confinement in the nanopores of silica matrix changed significantly from the bulk IL. The DFT-calculation in their work also indicated that the interaction of the IL with the surface resulted in changes in the vibrational bands. Another recent work has been devoted to a comprehensive study about the physicochemical properties and applications of the ILs confined in nanopores [38]. Singh et al. [39] considered the crystallization kinetics of pure IL [emim][BF_4] and IL confined in mesopores silica matrices. They found the significant influence of confinement on the crystallization rate and also crystallization dimensionality of IL. In another work, the same research group synthesized [emim][BF_4] confined in a silica matrix (ionogel) at different gelation temperatures and found that the rate of gelation was lower at lower temperatures [40]. Recently, another study by Singh et al. [41] demonstrated the formation of Si–O–S linkage along with the interaction of SiO_2–$[emim]^+$ cation and $SiOH–[ETSO_4]^-$ anion on confined IL [emim][$ETSO_4$] in silica nanopores matrix, both theoretically and experimentally.

The aim of this study was to investigate the structure and dynamic properties of the [emim][BF_4] IL inside interwall distances (from 10 to 28 Å) of an uncharged and nonpolar graphene via MD simulations. In the present work, effects of temperature in the range of 273 to 308 K on the properties of the confined IL were studied. In addition to temperature, confinement effects on the distribution of the cations and anions were examined. The paper was divided into the following parts: first, the simulation methods are described in "Computational details" section. Then, the results are presented and discussed by the illustration of radial distribution function, number of densities, diffusion, ionic conductivity, molar specific heat capacity at constant volume, and orientation of the ILs in "Results and discussion" section. Finally, concluding remarks are given in "Conclusions" section.

Computational details

In this work, MD simulations were performed using Tinker package (ver. 5.9) [42] to study the properties of the IL ([emim][BF_4]) confined between two graphene sheets. Figure 1a and b show the chemical structures and labeling scheme of the cation and anion of this IL, respectively. The interwall distances of two graphene sheets were H=(10, 14, 16, 20, 23, and 28) Å. The simulated systems consisted of 77 pairs of ions that were placed between two parallel graphene sheets. The experimental density of [emim][BF_4] is 1.294 gcm^{-3}. Although different interwall distances of the graphene sheets were chosen, the effective volume of the systems remained constant. Therefore, at a given temperature, density of the confined IL is constant. In other words, depending on the interwall distances of the graphene sheets, these numbers of pairs (77 cations and anions) were chosen to have the experimental density. Since the cation size of [emim][BF_4] was about 7.43 Å, the interwall distances of the graphene sheets from H=10 Å were considered and then these distances were increased from 10 to 28 Å in six steps. The IL was modeled using an OPLS-AA force field developed by Lopez et al. [43–47] and the parameters were taken from the previous studies [44–48]. The graphene surfaces, in this study, were uncharged and the dimensions of each elementary cell of the graphene surface were (2.46×4.26) $Å^2$. Additional details of these simulations are given in Table 1. It should be noted that seven different temperatures (278, 283, 288, 293, 298, 303, and 308) K were investigated. In the simulations, energy of the initial configurations was minimized; subsequently, the production run was performed by an NVT ensemble for all the temperatures. The temperature was controlled by a Nose'-Hoover thermostat [49] with the integration time step of 0.1 fs. The particle mesh Ewald was handled to carry out the long-range electrostatic interactions [50]; also, the short-range forces were calculated by the cutoff of 13 and 9 Å. The cross-correlation LJ parameters for the unlike atoms were computed using Lorentz–Berthelot combination rules [51]: $\sigma_{ij}=(\sigma_i+\sigma_j)^{1/2}$ and $\varepsilon_{ij}=(\varepsilon_i\varepsilon_j)^{1/2}$. The improved Beeman integration algorithm [52] was used to solve the equations of the motions with the time step of 1 fs. After the equilibrium time, the simulations were continued for another 12 ns. All the data and measured properties in each system were averaged during the last 2 ns of the simulation time.

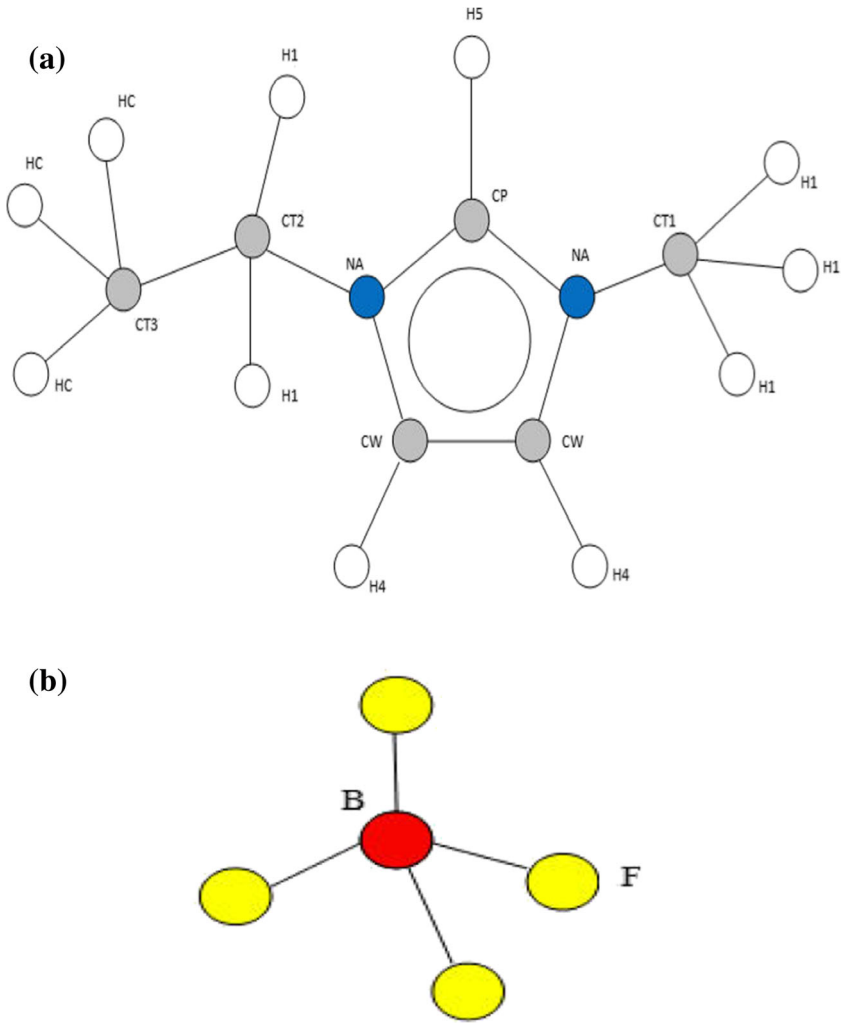

Fig. 1 Schematic representation and atom definitions for of ionic liquid 1-ethyl-3-methylimidazolium tetrafluoroborate. **a** The [emim] cation. **b** The [BF_4] anion

Results and discussion

Snapshots of confined systems

Snapshots of the simulated systems at 278 K are shown in Fig. 2a–c. The interwall distances were 28, 16, and 10 Å. Several layers of the anions and cations of [emim][BF_4] IL were observed at different interwall distances of the graphene sheets. These layering behaviors will be discussed in detail later (via the radial distribution functions and number density profiles). It can be seen that the cations and anions had a tendency to form aggregations around each other. In other words, a layer of the ions of opposite charges was formed around the same ions. Another layer of the ions of the opposite charges was also established around this layer; therefore, an aggregation of the IL was observed which grew throughout the cell. Aggregations of the IL were more compact at low distance between the two graphene sheets (H=10 Å).

Table 1 Simulation details for studied systems

Interwall distances (Å)	Number of elementary cell of the graphene surface	Total of atoms of two layers graphene sheet
10	32×7	1844
14	23×7	1340
16	20×7	1172
20	16×7	948
23	13×7	780
28	11×7	668

Time-average of potential energies

Figure 3a shows the average potential energy, E_{pot}, as a function of temperature at different distances between two graphene sheets. It can be seen that, except for H=10 Å, the magnitude of E_{pot} increased with increasing temperature from 278 to 308 K. The results showed that the average E_{pot} increased when distance increased from H=16 to 28 Å. Moreover, H=10 Å exhibited a maximum value of average E_{pot} because of very little distance between two graphene sheets and lack of free space in the direction perpendicular to the

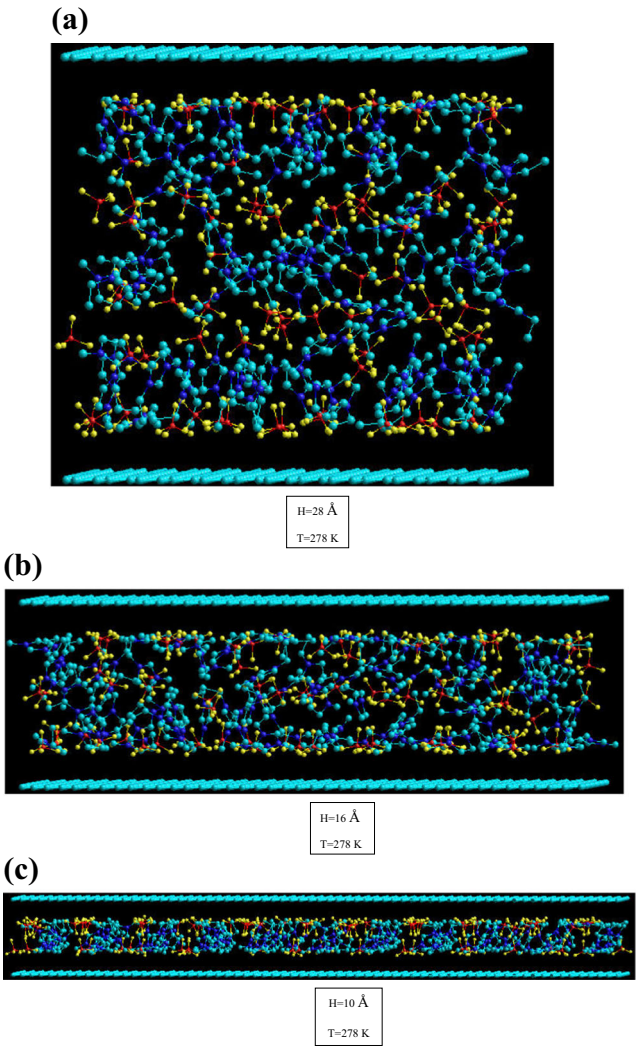

Fig. 2 Snapshots of [emim][BF_4] confined between two graphene sheets of different interwall distances at T=278 K. **a** H=28 Å. **b** H=16 Å. **c** H=10 Å. *Red*, *yellow*, *blue*, and *cyan spheres* correspond to boron, fluorine, nitrogen, and carbon atoms, respectively

graphene plates; therefore, non-bond covalant repulsive interactions and ionic interactions increased. Figure 3b shows the average E_{pot} as a function of the confinement distances at different temperatures. It can be observed that average E_{pot} decreased with an increase from low distances to H=16 Å and then increased with increasing distance. Therefore, the potential energies were minimum at H=16 Å.

Radial distribution functions (RDFs)

IL-IL RDFs

To understand the influence of the interwall distances and temperatures on the RDFs of ion-ion, the RDFs of anion-anion (B–B with solid line), anion–imidazolium ring of the cation (B–CP with dashed line), and anion–tail group of the cation (B–CT_3) in confined systems are shown in panels of

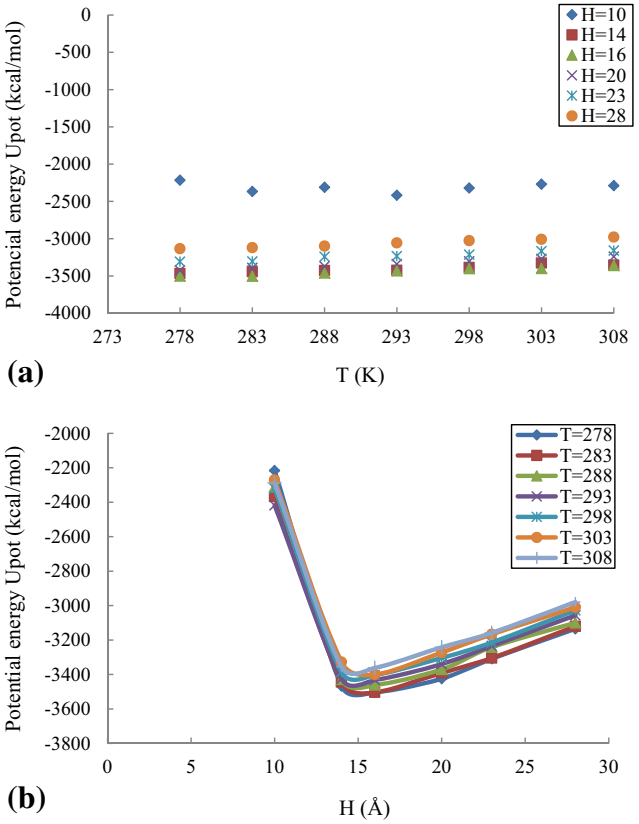

Fig. 3 **a** Temperature dependence of the potential energies at different distances between two graphene sheets; **b** Dependence of interwall distances of potential energies at different temperatures

Fig. 4a–b. These RDFs were at H=10 and 28 Å and T=278 K. As shown in Fig. 4a, the first and second peaks of the anion–anion interactions were around 4.05 and 4.55 Å. Intensity of the second peak was stronger and broader than that of the former. For the anion–imidazolium ring of the cation interactions (dashed line in Fig. 4a), two sharp peaks (at the distances of 3.35 and 5.56 Å, respectively) existed; the first peak showed higher intensity than the second one. Only a sharp and strong peak existed for the anion–tail group interactions at 4.15 Å. At H=10 Å, the comparison between the intensity and location of the interactions showed that the B–CP interactions were stronger than those observed for both anion–anion and anion–tail groups, as indicated by the height of the peaks. Because of the high tendency of the ring toward anion, a second layer was formed around anions (as shown in Fig. 4a). On the other hand, the anion–anion interactions were weak due to the repulsive interactions between anion and anion. It should be mentioned that the aggregation at small distances between two graphene sheets led to a strong ion–ion interaction. When the interwall distances increased from 10 to 28 Å (Fig. 4b), due to the increase of the available space for the movement of ions and decrease of the compactness of the ILs, height of the peaks decreased in each RDF. As illustrated in Fig. 4b, two weak peaks of the anion–anion RDF in Fig. 4a

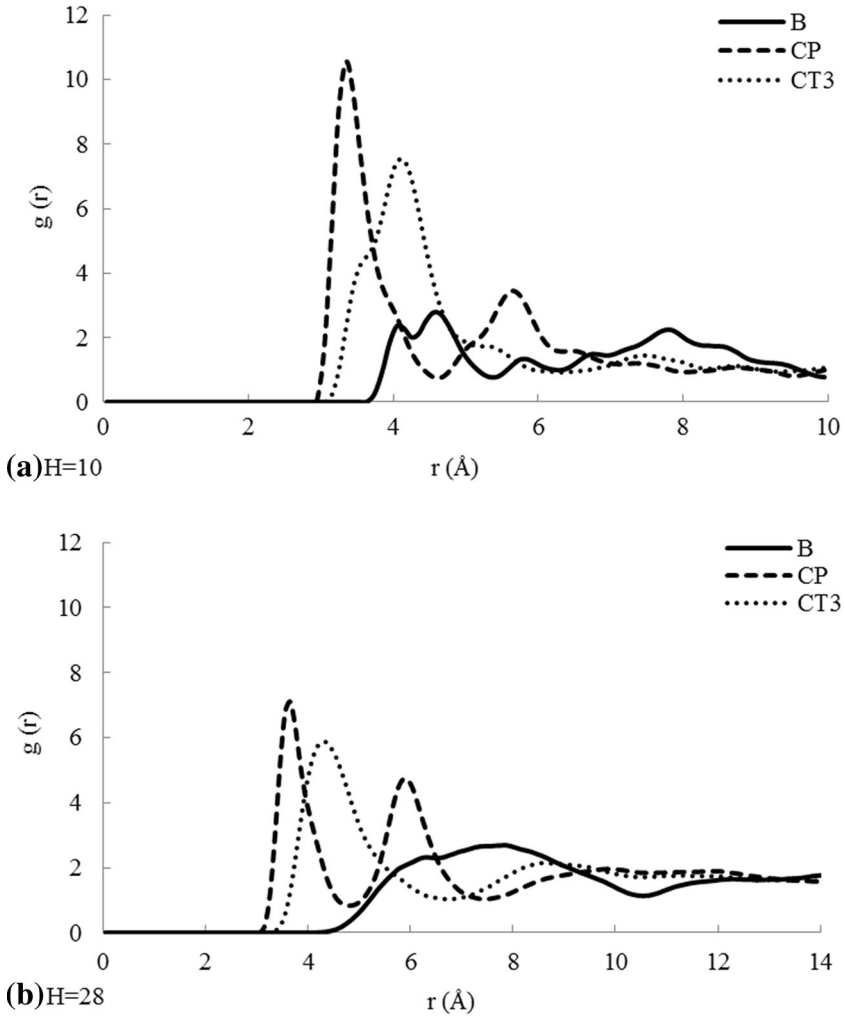

Fig. 4 RDFs of the anion–anion, anion–imidazolium ring of the cation, and anion–tail group of the cation at T=278 K. **a** The distribution at H=10 Å. **b** The distribution at H=28 Å

were merged together and formed a weak and board peak. This result could be understood using the snapshots mentioned in the text. The snapshots in Fig. 2a–c show that, with the increasing H, the IL aggregations were fairly separated. Therefore, anions had enough space to adjust their attraction and repulsion interactions with the graphene plane and different cation atoms. A comparison between Fig. 4a and b shows that the changes in the structure of IL aggregations led to the decreased height of the only peak in the anion–tail group distribution (in Fig. 4b, the position of this peak is at 4.35 Å) and the decrease of the first peak and increase of the second peak in the anion–ring distributions (in Fig. 4b, these peaks appear at 3.65 and 5.85 Å, respectively). All three investigated atoms had the same size and were attached to a hydrogen atom; therefore, location of the peaks can be considered as a measure of the tendency of different investigated groups. It was also observed that the first peak of B–CP RDFs appeared at smaller distances and thus the group ring of the cation was closer to the anion. On the other hand, the B–B RDFs appeared at larger distances due to ionic anion-anion repulsiveness. Distributions of the B–B and B–CP at other temperatures and interwall distances are shown in Figs. S1 and S2 of Supporting information, respectively.

Graphene–IL RDFs

For better understanding of the structural properties, the profiles of RDFs for distances between C atoms of graphene and B atoms of the anion (C–B), and also between C atoms of graphene and CP (C–CP) and CT3 (C–CT3) atoms of the cation are displayed in Fig. 5a–c at different distances between two graphene sheets at 278 K, respectively. RDFs for the graphene–anion at other temperatures are shown in Fig. S3 of Supporting information (C–CP and C–CT3 distributions are not shown). The first peak of C–B RDFs (Fig. 5a) appeared at 3.85 Å (for H=10 Å) and 4.25 Å (for other wall separations). As H increased from 10 to 23 Å, the height of these peaks started to decrease. This observation clearly indicated the aggregations of the ILs at smaller distances. Aggregation behavior of the ILs led to intense repulsion among the same ions; therefore, the anions tended toward the graphene walls at lower wall distances. These conclusions were

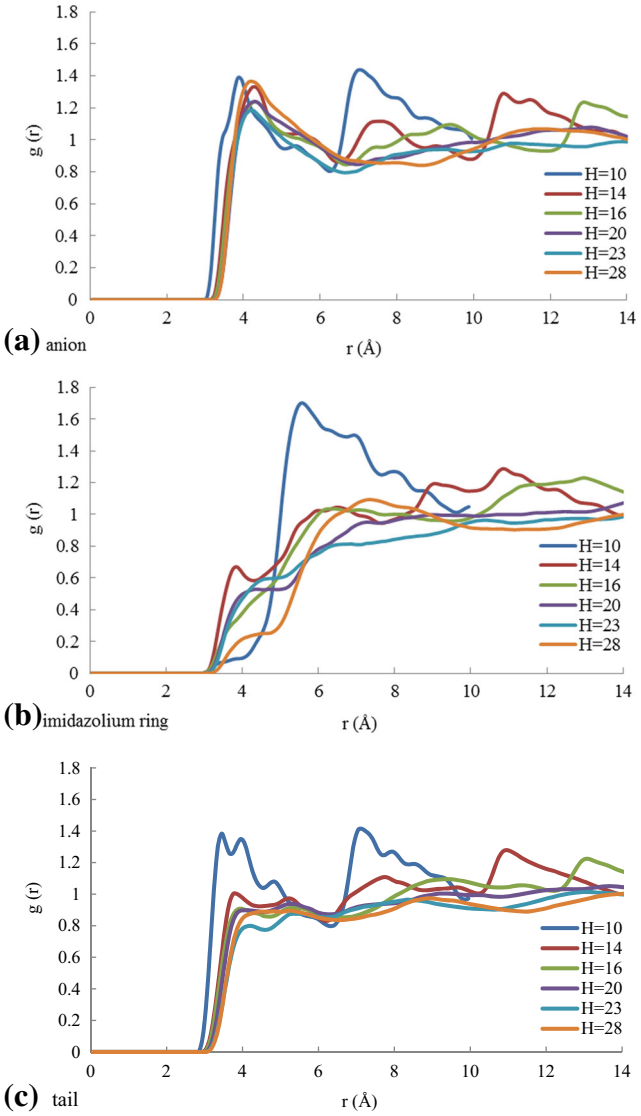

Fig. 5 RDFs of the graphene–IL of different distances between two graphene sheets at T=278 K. **a** A graphene–anion distribution, **b** A graphene–imidazolium ring distribution, and **c** A graphene–tail distribution

reinforced by shorter distances of the peaks at the lower distances between the two graphene sheets in Fig. 5a. When the distance between the two graphene sheets increased, there was enough space for the adjustment of repulsion and attraction forces. Appearance of the second and third peaks indicated a layer structure of the ILs between the two sheets. As the distance between the two graphene sheets increased, the intensity and height of these peaks started to decay, similar to the first peak. The above-mentioned results confirmed the effect of the available space and aggregation of the ILs on the intensity of the peaks. In Fig. 5b and c (C–CP and the C–CT_3 RDFs, respectively), there were weak and broad peaks. In Fig. 5b, intensity of the former peaks was less than that of the latter ones and an inverse trend was observed in Fig. 5c. These results provided information about the preferred distributions of the cations around the graphene, suggesting that a greater number of the ILs tended to interact primarily with the graphene from alkyl chain side (graphene–alkyl chain interactions were stronger than π-cation interactions). The comparison between Fig. 5b and c shows that the tail group of the cation appeared at smaller distances and, therefore, was closer to the graphene. Furthermore, as can be seen in these representations, height of the peaks decreased with increasing the distance between the two graphene sheets. Similar to Fig. 5a, intensity of the peak corresponding to H=28 Å was higher than the observed one for H=23 Å. Also, increase at the confinement distances caused disappearing height and intensity of the second and third peaks. The RDFs corresponding to the C–CP and C–CT_3 at other temperatures were similar to those shown in Fig. 5b and c; thus, they were not shown. Also, RDFs of the bulk were not given.

Potential of mean force

To investigate the different contributions wall/liquid and liquid/liquid, we have calculated radial PMFs W(R) to illustrate these contributions:

$$W(R) = -kTlog\ g(r) \quad (1)$$

where g(r) is the radial distribution function. PMFs between carbon atoms of graphene and B atoms of IL (gra–B) and also between carbon atoms of graphene and tail group of IL (gra–tail) at different distances between two graphene sheets were calculated and shown in Fig. 6a and b. Also, PMFs of anion–anion (B–B), anion–imidazolium ring of the cation (B–CP), and anion–tail group of the cation (B–CT_3) in one confined system (H=28 Å) and bulk are shown in Fig. S4 of the Supporting information. As shown in Fig. 6a and b, at all H, the potential energy was totally reduced and attractive regimes became more apparent. At H=10 Å, there was stronger interaction between graphene and IL atoms compared to other H. Moreover, at H=10 Å, more than one minimum of the energy can be seen.

Number density profiles of the cation and anion

In order to study the structures at different distances and T= 278 K, the number density profiles of the anions and cations along the distance between the two graphene sheets were calculated and shown Fig. 7a–c. Thus, the number densities of CP atoms of the ring, B atoms of the anion, and the terminal carbon atoms of the alkyl group were calculated for H=28, 16, and 10 Å. In all the profiles, the dense layers of the IL near the graphene surfaces were observed due to strong interactions between the graphene and [emim][BF_4], as reflected by the positions and heights of the first peaks (see arrows in Fig. 7).

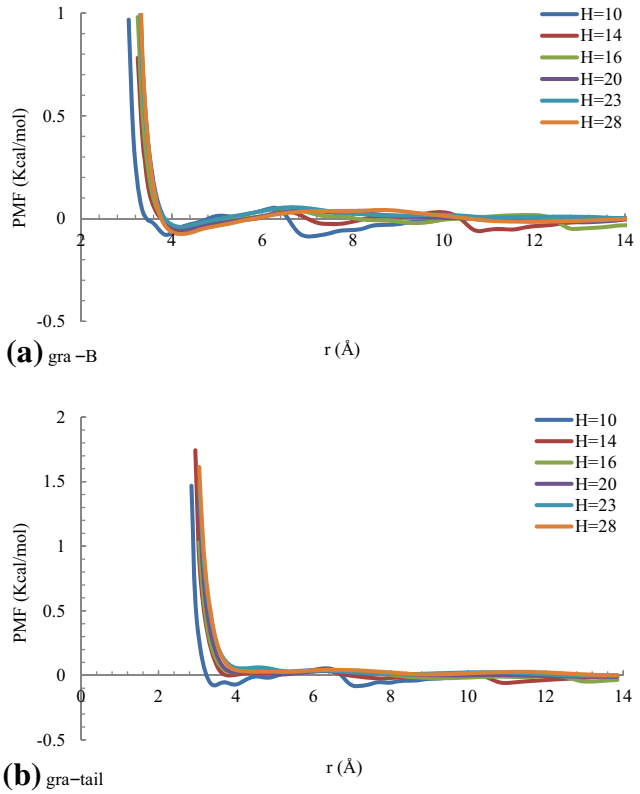

Fig. 6 PMFs of the graphene and [emim][BF_4] at different distances between two graphene sheets. **a** gra–B, and **b** gra–tail. Temperature is 278 K

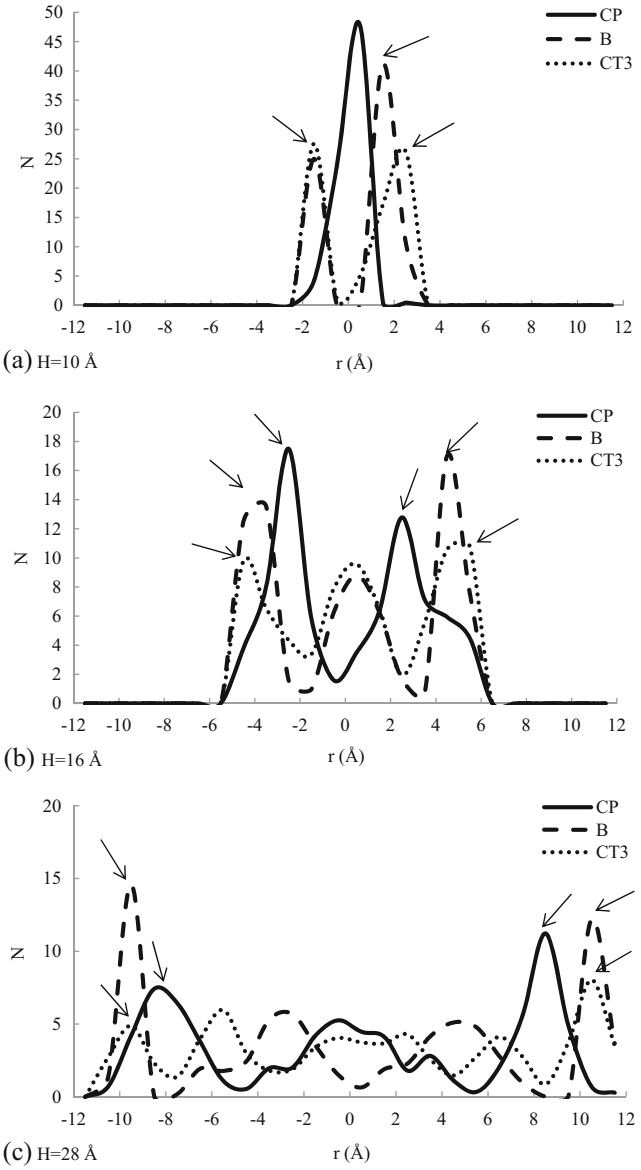

Fig. 7 Number density profiles of B, CP, CT_3 atoms for [emim][BF_4] confined between two graphene sheets of different interwall distances at T=278 K. **a** H=10 Å, **b** H=16 Å, and **c** H=28 Å. The *arrows* indicate the dense layers of IL

These behaviors have been seen in many other simulation studies [42, 53–55]. A striking feature from these profiles was similar distribution of the anion and the tail group of the cation. Compared with CP atom, the tail group of the cation was slightly close to the walls of the graphene. At low interwall distances, the density distribution showed higher peaks. Height of the peaks in density profiles decreased when the distance between the two graphene sheets increased. In addition, the number of the layers of the cation and anion increased as H increases. According to Figs. 2c and 7a (H= 10 Å), the density profiles for both anion and tail groups showed two peaks (bilayer) near the walls of the graphene, whereas the distribution of CP atom was monolayer, sharp, and at the center. Moreover, it can be seen that the intensity of the two peaks was different for the anion; however, the intensity of the peaks of the tail group of the cation was almost similar and half of the intensity of one peak of the ring. At H= 16 Å, according to Figs. 2b and 7b, the density profiles of the anion and tail group were three-layered, whereas for the ring group of the cation, the two central and terminal peaks were merged together. CP atoms were distributed into two layers that were among the three layers of B and CT3 atoms. In other words, a five-layered distribution can be seen in H=16 Å, one of which belonged to CT3 and B atoms together and another belonged to CP atom alternatively. Another striking feature in this distribution was that there was no overlapping between B and CT3 atoms with CP atom and, therefore, anions and cations had maximum independence. According to Figs. 2a and 7c at H=28 Å, the overlap between B and CT3 atoms decreased in the middle layers. B and CT3 atoms were distributed into four layers. At the center, due to the bulk behavior, sharp peaks were not seen. Two sharp peaks next to the walls of the graphene indicated that CP atoms were distributed into two layers. According to these presentations, it can be seen that both anion and tail group tended to remain in the regions near the graphene walls, as indicated by the heights of the peaks. Density profiles of the anion and those at other

interwall distances are shown in Fig. S5 of Supporting information.

Dynamic properties

For obtaining diffusion coefficients of ions (D_i), the mean-square displacement ($\langle|r_i^{cm}(t)-r_i^{cm}(0)|^2\rangle$) of the cation and anion was calculated and then:

$$D_i = lim_{t\to\infty}(1/6t)\frac{\left\langle\left|r_i^{cm}(t)-r_i^{cm}(0)\right|^2\right\rangle}{dt} \quad (2)$$

Diffusion coefficients of the cations and anions as a function of temperature at different confinement distances are shown in Fig. 8a and b, respectively. Diffusion coefficients of the ions as a function of H at different temperatures are also shown in Fig. 8c and d. For all the studied confinement distances, diffusion of the cations was higher than that of the anions. Higher diffusion of the cation was consistent with that of other works [56, 57]. Effects of temperature and H were clearly observed on the diffusion of the ions. As can be seen, the diffusion values of the ions increased as the temperature and distances between the two graphene sheets increased. An increase in the temperature leads to an increase in the mobility and movement of ions, and an increase in H suggested a decrease in the number of collisions per unit volume. Thus, these two factors led to increased diffusion of ions. Figure 8c and d indicate that the slope of these curves increased at H= 16 Å. The important features for notice were the diffusion gap between H=14 and 16 Å and slope changes between T=283 and 288 K. An understanding of diffusion behaviors of the anions and cations adsorbed on the graphene surface can be obtained from the calculation of activation energy using the Arrhenius relation, as follows:

$$D = D_0\ \exp(-E_a/kT) \quad (3)$$

where T is temperature, K is Boltzmann constant, $D_0$is pre-exponential factor, and E_a is activation barrier for surface diffusion of ions. The results obtained from Arrhenius plot of the surface diffusion coefficients (ln D profiles as a function of 1/T) indicated a linear behavior at different temperatures as the characteristic behavior of the Arrhenius. So, using coefficient diffusions of the ions, E_a was calculated. Figure 9 shows E_a as a function of different distances between two graphene sheets. As shown in Fig. 9, the barrier energies for both anions and cations decreased as the distance between two graphene sheets increased. Furthermore, the slope of this curve as a function of H decreased at H=16 Å. Pre-exponential factors as a function of H are shown in Fig. S6 of Supporting information. As can be observed, D_0 values increased with increasing H.

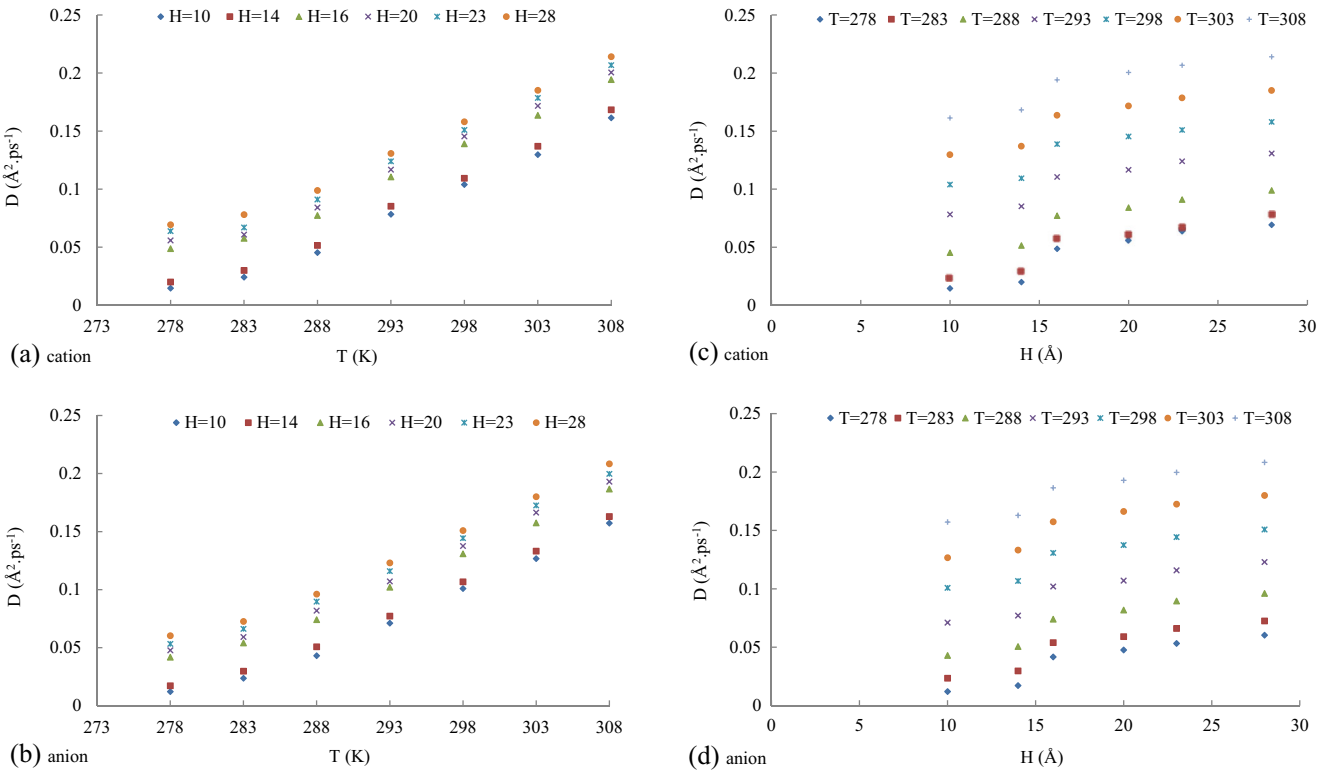

Fig. 8 Diffusion coefficients of the cation and anion of [emim][BF_4]. **a** Diffusion at different temperatures. **b** Diffusion at different distances between two graphene sheets

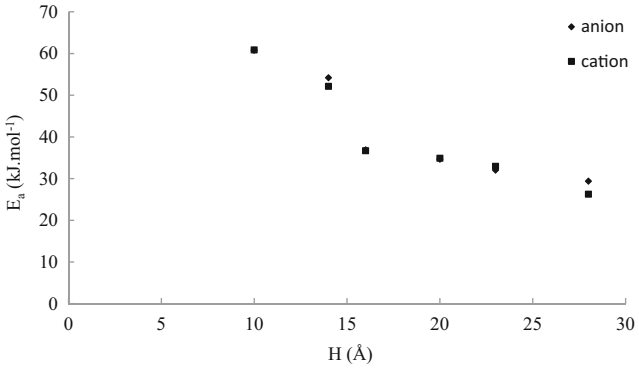

Fig. 9 **a** Activation energies for both anion and cation as a function of H

Constant-volume heat capacity

Figure 10a and b show the constant-volume heat capacity, C_v, of the studied IL as a function of H and temperature, respectively. C_v was calculated as follows:

$$C_v = \frac{1}{KT^2}\left\langle (\delta E)^2 \right\rangle \tag{4}$$

where $\delta E = E - \langle E \rangle$ and E is the internal energy. In both figures, the molar heat capacity at constant volume indicated an increasing trend; however, in some cases, a different trend was obsereved.

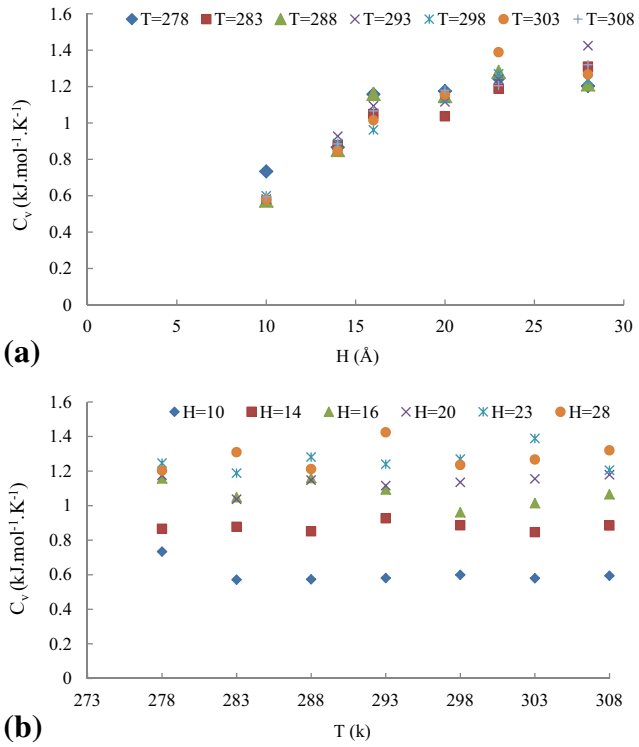

Fig. 10 Molar specific heat capacity at constant volume for studied systems. **a** At different temperatures. **b** At different distances between two graphene sheets

Orientation of the ring of the cation

To investigate the cation configuration of the orientational preferences, the second order Legendre polynomial [54] given was calculated:

$$P_2(\theta) = \left(\frac{1}{2}\left(3cos^2\theta - 1\right)\right) \tag{5}$$

where θ is the angle between the surface of graphene and plane of the aromatic ring of the IL [58]. For isotropic distribution, the function's value was 0. For parallel and perpendicular distributions, its value attains 1 and −0.5, respectively. It should be mentioned that, in symmetric ILs, these orientational preferences are reduced. $P_2(\theta)$ of the cations as a function of H is shown in Fig. 11. These results showed the orientational preference of the ring at all different distances between two graphene sheets. That is, a large fraction of the ring plane preferred to lie flat on the graphene surface. This preference configuration of the cation was consistent with results of other works [55]. At H=10 and 28 Å, most of the ILs were parallel to the graphene surface. These parallel orientations were fewer at H=16 Å, i.e., orientation of the ILs was close to isotropic distribution at these interwall distances of the graphene.

Conclusions

Structural and dynamic properties of [emim][BF_4] confined between two walls of the graphene at 278 to 308 K were studied via MD simulations. The distances between the two graphene sheets were (10, 14, 16, 20, 23, and 28) Å. The present results indicated that a layering behavior of the anion and cation was observed for the [emim][BF_4] at different distances between two graphene sheets. Also, cations and anions tended to form aggregations around each other. In addition, these results demonstrated that the diagram of potential energies as a function of H had a minimum at H=16 Å. The number density profiles showed the dense layers of the IL near

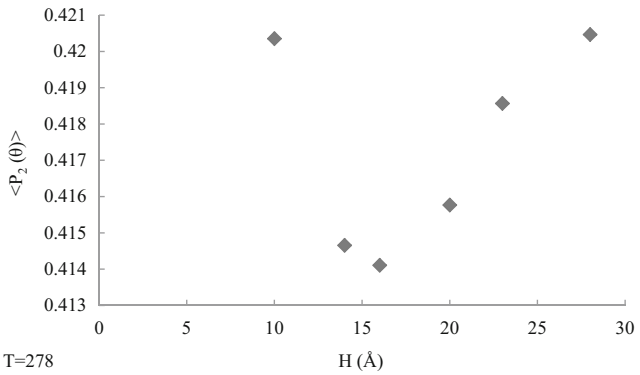

Fig. 11 Calculated $P_2(\theta)$ of the [emim] cation as a function of distances between two graphene sheets

the graphene surfaces, due to strong interactions between the graphene and [emim][BF_4]. Also, density profiles of the IL at H=16 Å had minimum overlap of the atoms of the cations and anions. In comparison with CP atom, the tail group of the cation was close to the walls of the graphene. The diffusion coefficients calculated from the mean-square displacements indicated that the diffusion of the cations was higher than that of the anions (for all the studied confinement distances). The diffusion values of the cations and anions increased as the temperature and distances between the two graphene sheets increased. Also, the diffusion gap between H=16 and 14 Å and slope changes between 283 and 288 K were observed. Increasing the temperature and H resulted in an irregular trend of increase in the molar heat capacity of the ions. Finally, the second order Legendre polynomial function showed that the ring plane of the cation was flat on the graphene surface at all distances between the two graphene sheets.

References

1. Leng Y, Cummings PT (2005) Phys Rev Lett 94:026101
2. Calbi MM, Cole MW, Gatica SM, Bojan MJ, Stan G (2001) Rev Mod Phys 73:857
3. Alcoutlabi M, McKenna GB (2005) J Phys Condens Matter 17: R461
4. Rogers RD, Seddon KR, Volkov S (eds) (2002) Green industrial applications of ionic liquids. NATO Science Series. Kluwer, Boston
5. Wasserscheid P, Welton T (eds) (2002) Ionic liquids in synthesis. Wiley-VCH, Weinheim
6. Simon P, Gogotsi Y (2008) Nat Mater 7:845
7. Hagfeldt A, Boschloo G, Sun L, Kloo L, Pettersson H (2010) Chem Rev 110:6595
8. Kamat PV (1906) Acc Chem Res 2012:45
9. Brennecke JF, Maginn EJ (2001) AICHE J 47:2384
10. Welton T (1999) Chem Rev 99:2071
11. Aliaga C, Santos CS, Baldelli S (2007) Phys Chem Chem Phys 9: 3683
12. Sloutskin E, Ocko BM, Tamam L, Kuzmenko I, Gog T, Deutsch M (2005) J Am Chem Soc 127:7796
13. Bhargava BL, Balasubramanian S (2006) J Am Chem Soc 128: 10073
14. Heggen B, Zhao W, Leroy F, Dammers AJ, M ller-Plathe F (2010) J Phys Chem B 114:6954
15. Sieffert N, Wipff G (2008) J Phys Chem C 112:19590
16. Mezger M, Schröder H, Reichert H, Schramm S, Okasinski JS, Schröder S, Honkimäki V, Deutsch M, Ocko BM, Ralston J, Rohwerder M, Stratmann M, Dosch H (2008) Science 322:424
17. Lynden-Bell RM, Kohanoff J, Del Popolo MG (2005) Faraday Discuss 129:57
18. Chaumont A, Schurhammer R, Wipff G (2005) J Phys Chem B 109:18964
19. Kislenko SA, Samoylov LS, Amirov RH (2009) Phys Chem Chem Phys 11:5584
20. Wang S, Li S, Cao Z, Yan T (2009) J Phys Chem Chem Phys 11: 5584
21. Ghatee MH, Moosavi F (2011) J Phys Chem C 115:5626
22. Dou Q, Sha M, Fu H, Wu G (2010) Chem Phys Chem 11:2438
23. Maolin S, Fuchun Z, Guozhong W, Haiping F, Chunlei W, Shimou C, Yi Z, Jun H (2008) J Chem Phys 128:134504
24. Song Y, Qu K, Zhao C, Ren J, Qu X (2010) Adv Mater 22:2206
25. Chen F, Qing Q, Xia J, Li J, Tao N (2009) J Am Chem Soc 131: 9908
26. Ariga K, Hill JP, Ji Q (2007) Phys Chem Chem Phys 9:2319
27. Ji Q, Honma I, Peak SM, Akada M, Hill JP, Vinu A, Ariga K (2010) Angew Chem Int Ed 49:9737
28. Ariga K, Ji Q, Hill JP, Bando Y, Aono M (2012) NPG Asia Mater 4:1
29. Xiao W, Sun Z, Chen S, Zhang H, Zhao Y, Huang C, Liu Z (2012) RSC Adv 2:8189
30. Rajput NN, Monk J, Hung FR (2012) J Phys Chem C 116:14504
31. Shim Y, Kim HJ, Jung Y (2012) Faraday Discuss 154:249
32. Rajput NN, Monk J, Hung FR (2014) J Phys Chem C 118:1540
33. Singh R, Monk J, Hung FR (2010) J Phys Chem C 114:15478
34. Sha M, Wu G, Liu Y, Tang Z, Fang H (2009) J Phys Chem C 113: 4618
35. Pinilla C, Del Popolo MG, Lynden-Bell RM, Kohanoff J (2005) J Phys Chem B 109:17922
36. Holbrey JD, Seddon KR (1999) J Chem Soc Dalton Trans pp 2133-2140, doi: 10.1039/A902818H
37. Gupta AK, Singh MP, Singh RM, Chandra S (2012) Dalton Trans 41:6263
38. Singh MP, Singh RK, Chandra S (2014) Prog Mater Sci 64:73
39. Gupta AK, Singh RK, Chandra S (2014) RSC ADV 4:22277
40. Gupta AK, Singh RK, Chandra S (2013) RSC ADV 3:13869
41. Gupta AK, Verma YL, Singh RK, Chandra S (2014) J Phys Chem C 118:1530
42. Won CY, Joseph S, Aluru NR (2006) J Chem Phys 125:114701
43. Jorgensen WL, Maxwell DS, Tirado-Rivers J (1996) J Am Chem Soc 118:11225
44. Lopes JNAC, Deschamps J, Pádua AAH (2004) J Phys Chem B 108:2038
45. Lopes JNAC, Pádua AAH (2004) J Phys Chem B 108:16893
46. Lopes JNAC, Pádua AAH (2006) J Phys Chem B 110:19586
47. Lopes JNAC, Padua AAH, Shimizu K (2008) J Phys Chem B 112: 5039
48. Liu Z, Huang S, Wang W (2004) J Phys Chem B 108:12978
49. Hoover WG (1985) Phys Rev A 31:1695
50. Darden T, York D, Pedersen L (1993) J Chem Phys 98:10089
51. Allen MP, Tildesley DJ (1987) Computer simulation of liquids. Clarendon, Oxford
52. Beeman D (1976) J Comput Phys 20:130
53. Wang S, Li S, Cao Z, Yan T (2010) J Phys Chem C 114:990
54. Senapati S, Chandra A (1998) Chem Phys 231:65
55. Gao J, Luedtke WD, Landman U (1997) J Phys Chem B 101:4013
56. Margulis CJ, Stern HA, Berne BJ (2002) J Phys Chem B 106:12017
57. de Andrade J, Böes E, Stassen H (2002) J Phys Chem B 106:13344
58. Foroutan M, Mohammadi M (2013) Phys Chem Chem Phys 15: 2482